Appl. Phys. B 67, 275–282 (1998)

Applied Physics B
Lasers
and Optics

In-situ sensing of tropospheric water vapor using an airborne near-IR diode laser hygrometer

D.M. Sonnenfroh[1], W.J. Kessler[1], J.C. Magill[1], B.L. Upschulte[1], M.G. Allen[1], J.D.W. Barrick[2]

[1] Physical Sciences Inc., 20 New England Business Center, Andover, MA 01810-1077, USA
(Fax: +1-978/689-3232, E-mail: sonnenfroh@psicorp.com, kessler@psicorp.com, magill@psicorp.com, upschulte@psicorp.com, allen@psicorp.com)
[2] NASA Langley Research Center, Hampton, VA 23681, USA
(Fax: +1-757/864-5841, E-mail: j.d.barrick@larc.nasa.gov)

Received: 31 March 1998/Revised version: 3 June 1998

Abstract. We describe a near-IR diode laser hygrometer developed for in-situ measurement of water vapor from airborne platforms throughout the troposphere. The sensor is based on the absorption of a 1.39-μm diode laser beam and employs an open, folded 50-cm absorption path placed in the free-stream air using an external probe. Water vapor number density is continuously recorded at 10 Hz. Extensive laboratory testing showed a sensitivity of 10^{12} molecules cm^{-3} $Hz^{-1/2}$ (signal-to-noise ratio 3). This is equivalent to a mixing ratio of 0.3 ppmv at average midlatitude tropopause conditions or a mixing ratio of 0.6 ppmv under boundary-layer conditions. The corresponding minimum measurable absorbance is 10^{-5} $Hz^{-1/2}$. The laser hygrometer was field-demonstrated aboard the NASA P3B research aircraft, during a series of flights spanning several weeks in the summer of 1997. During this demonstration, the laser hygrometer was intercompared with two optical chilled mirror hygrometers. In general, the laser hygrometer performed well; however, under some conditions, it reported water vapor number densities 20% greater than the cryogenic frost-point hygrometer. This difference is currently under study.

PACS: 07.65; 33.00; 42.80

An important component of many current atmospheric field measurement programs is the quantification of the spatial and temporal variability of water vapor. Water vapor has both direct and indirect radiative feedbacks to climate which can vary with altitude. Water vapor is the most abundant greenhouse gas; its concentration altitude profile is a component in determining heating and cooling rates [1]. Water vapor also figures directly in the formation, persistence, and dissolution of clouds. While half of all water vapor in the atmosphere resides in the troposphere below 850 mb (∼ 1.5 km), only about 10% is above 500 mb (∼ 5.5 km) [2]. Although less than about 1% is found in the stratosphere, changes in the water vapor mixing ratio there can have significant impacts on radiative forcing of climate [2, 3]. In addition, water vapor is reactive and participates in several important chemical cycles. Its lifetime is about 10 days, which implies that it is both spatially (horizontally and vertically) and temporally inhomogeneous [1]. Measurement at many places (latitude, longitude, altitude) and times is necessary then to achieve a valid database.

Water vapor is currently measured in situ with several different sensors, including the Lyman-alpha photometer, the dew/frost-point optical chilled mirror (OCM) hygrometer, and thin-film capacitors [4]. Thin-film capacitance sensors have reasonably good accuracy and sensitivity. Recent research, however, has revealed problems with sensitivity and accuracy at both low and high relative humidities (RH) at altitudes corresponding to the tropopause (10 to 12 km) [4]. At the low temperatures characteristic of the tropopause, the temporal response of thin-film capacitance sensors also degrades. They can suffer from drift (arising from changing temperature) and poisoning. The Lyman-alpha photometer uses vacuum ultraviolet light from an H_2 lamp (the Lyman-α line at 121 nm) to dissociate H_2O. Emission from the excited OH dissociation product is then detected. The technique can suffer from chemical interference. The VUV emission is sufficiently energetic to dissociate other species in the sample to produce excited OH directly. In addition, the calibration of the instrument involves assuming a fixed quenching rate of OH, which may vary with changing atmospheric conditions. Surface acoustic wave (SAW) quartz crystal microbalance sensors, while fairly new, possess high sensitivity and fast temporal response. This technology may be sensitive to surface contamination effects, however. State-of-the-art chilled mirror hygrometers can measure frost points as low as about −90 °C, use Stirling cycle coolers to regulate the temperature of the mirror, are compact, and are energy efficient [5]. Frost-point accuracies of ±0.5 °C can be achieved. This corresponds to a number density accuracy of about 5% at −80 °C and about 10% at −90 °C. Instrument response times can be as fast as 1 s. Proper design and maintenance procedures are needed, however, to minimize eventual mirror contamination, to minimize overshoot on sampling low-to-high humidity transients, and to minimize recovery time on wetting [4]. Problems measuring very low water vapor concentrations

with OCMs are well known, as is the potential for supercooling of the liquid water film on the mirror (for temperatures greater than −40 °C).

The goal of this work was to develop a new water vapor sensor with enhanced performance capabilities compared to existing sensors, that could be routinely deployed on a research aircraft and which would be capable of making high-precision measurements of water vapor throughout the troposphere. We have designed, developed, and field-tested a near-IR tunable diode laser absorption spectrometer to meet this need. Near-IR diode lasers have been developed into rugged and reliable light sources by the telecommunications industry. Stable, single-longitudinal-mode devices of useful output power (∼ 10 mW) are readily available at a variety of wavelengths between 0.7 and 2 μm. The frequency output of these lasers can be modulated via the injection current which enables high measurement rates. When coupled with an ultrasensitive detection technique, diode laser absorption spectrometers are capable of making near-shot-noise-limited absorption measurements. Peak absorbances as small as 1×10^{-5} can be routinely measured under field conditions. Our near-IR tunable diode laser hygrometer detects water vapor via absorption of a strong, isolated line at 7181.172 cm^{-1} (1.3925 μm) in the $\nu_1 + \nu_3$ combination band. This line was chosen to maximize sensitivity and minimize the required optical pathlength. This is among the strongest lines in the water spectrum between 1.3 and 2.0 μm. A model spectrum of the region of interest as calculated using the HITRAN database [6] is presented in Fig. 1. In addition, our laser hygrometer employs an external measurement path, instead of extractive sampling, to enable true in situ sampling.

Research-grade versions of mid-IR tunable Pb-salt diode laser spectrometers have been developed for water [7] and have been flown on several aircraft, such as NASA's high-altitude ER-2 research aircraft [8, 9]. Currently, two of NASA's instruments are being downsized for deployment on unmanned aerial vehicles (UAVs) [10]. These instruments use frequency modulation (FM) detection techniques and achieve high sensitivity by using long optical pathlengths. While mid-IR diode laser sensors have sufficient sensitivity for measurement of water vapor to the tropopause, they are less attractive than near-IR diode laser sensors for routine aircraft deployment because of complex laser tuning behavior, size, and need for cryogenic cooling. Two other airborne, near-IR diode laser sensors for H_2O vapor have recently been demonstrated. Silver and Hovde have developed an airborne diode laser hygrometer operating at 1.31 μm [11]. Extractive sampling into an absorption cell housing a folded 25-m optical path is used along with wavelength modulation spectroscopy detection to achieve a sensitivity of 8 ppmv. Collins et al. are developing a near-IR diode laser hygrometer that uses an external sampling path [12].

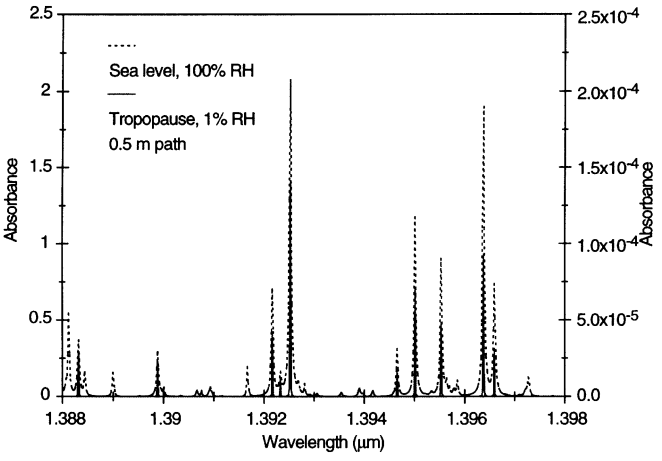

Fig. 1. Model HITRAN water vapor absorption spectrum near 1.39 μm. Absorption per meter pathlength is presented under both sea level (1013 mB, 300 K, saturated) and extreme tropopause (∼ 15 km, 120 mB, 190 K, 0.2 ppmv) conditions

1 Sensor performance

In contrast to the near- and mid-IR diode laser sensors mentioned above, which use frequency modulation (FM) detection techniques, our laser hygrometer achieves near-shot-noise-limited absorption measurements by using a balanced ratiometric detection (BRD) technique. This novel electronic noise-canceling technique was originally developed at IBM [13–15] and further refined at PSI for small absorbance measurements of atmospheric trace species [16]. The general experimental setup is illustrated in Fig. 2. In this dual-beam technique, the diode laser beam is split into signal and reference beams. Cancellation of excess laser amplitude noise is achieved by balancing the photocurrents from each photodiode. This balance is achieved electronically with the BRD, in contrast to the more familiar optical intensity balance of dual beam spectrometers. Common mode laser noise in the two channels is reduced by more than 50 dB, or 5 orders of magnitude enabling near-shot-noise-limited absorption measurements. Noise reduction to the shot-noise limit has been demonstrated both by Hobbs [13–15] and by PSI [16]. We have routinely used the BRD in field demonstrations to measure peak absorbances as low as 10^{-5}.

The ratiometric response of the BRD is given by

$$V_{\log} = G \ln\left(\frac{I_{\mathrm{ref}}}{I_{\mathrm{sig}}} - 1\right), \tag{1}$$

where G is the fixed gain of the internal integrating amplifier. Substituting Beer's law for $I_{\mathrm{ref}}/I_{\mathrm{sig}}$ in (1) produces the relationship between $V_{\log}$ and the absorbance, α:

$$V_{\log} = G \ln\left[B\mathrm{e}^{\alpha} - 1\right], \tag{2}$$

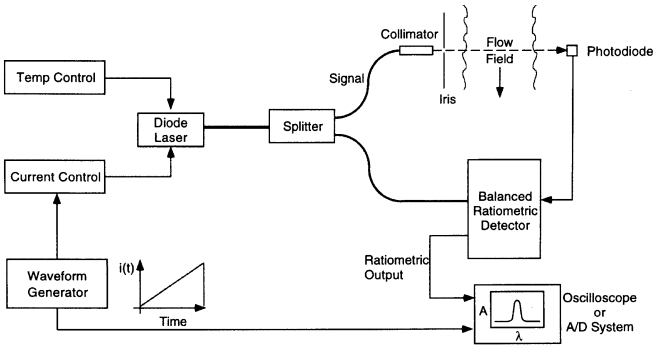

Fig. 2. Schematic of laser hygrometer architecture

where B is the ratio of $I_{\mathrm{ref}}/I_{\mathrm{sig}}$ away from any absorption. The absorbance is given by:

$$\alpha(\nu) = S(T)g(\nu, \nu_0, T, p)N\ell\,, \tag{3}$$

where $S(T)$ is the linestrength, $g(\nu, \nu_0, T, p)$ is the lineshape, N is the number density, and ℓ is the pathlength. In the limit of small absorbance, the absorbance at a given frequency is calculated from $V_{\log}$ as

$$\alpha = \frac{u}{u+1}\frac{V_{\log}}{G}\,. \tag{4}$$

Here, u is the balance signal and equals $B-1$ and G is the instrument gain factor. Finally, the number density is determined by integrating the absorbance across the lineshape:

$$N = \frac{\int \alpha(\nu)\,\mathrm{d}\nu}{S(T)\ell} = \frac{1}{S(T)\ell}\frac{u}{u+1}\frac{1}{G}\sum V_{\log}\delta\nu\,. \tag{5}$$

In practice, the integral is approximated by using a Simpson's rule summation. The differential frequency element, $\delta\nu$, is measured in the lab by using a confocal Fabry–Pérot interferometer (spectrum analyzer) for the scan range over which the sensor operates.

The wide dynamic range of the hygrometer arises from using a very strong, isolated water absorption line along with a more exact development of the BRD response, using a full inversion of Beer's law, applicable to all absorption regimes. The strong absorption line enables high sensitivity for low water vapor mixing ratios for measurements at the tropopause. The extended treatment of the BRD response is needed to recover number densities when the absorption is high (optically thick), which can occur at large water vapor mixing ratios for measurements in the boundary layer.

Both the linestrength, S, and the lineshape function, g, depend on the gas temperature with g depending on the pressure as well. For atmospheric measurements, both pressure and temperature vary with altitude. By scanning the laser frequency across the entire absorption lineshape, the pressure dependency of the lineshape function is removed from the measurement. While the full temperature dependence of the linestrength is used in the reduction of signals to number density, a line for which the linestrength has a minimal temperature dependence is typically chosen for use. Scanning fully resolved absorption lineshapes also reduces interferences from broadband absorbers in the background gas and nonresonant scattering from aerosols.

We calibrated the BRD by making a series of absorption measurements over several orders of magnitude of water concentration. The calibration experiment was performed by adding water vapor to an absorption cell. For each water vapor concentration, the BRD log voltage and the signal and reference linear voltages were recorded for the entire laser scan. Equations (3) and (4) are used to solve for N in terms of the known water vapor linestrength, the lineshape function, the pathlength, and the measured quantities u and $V_{\log}$. G is then determined by a linear least-squares fit of the calculated number densities to the values measured by the calibrated capacitance manometers. (In this work, the laser spectral bandwidth (approximately 100 MHz, determined using a spectrum analyzer) has been deconvolved from the measured lineshapes.) The data and corresponding fit are shown in Fig. 3. A linear relationship is observed between the laser hygrometer concentrations and the capacitance manometer concentrations over approximately three orders of magnitude. There is a slight deviation from linearity at high water vapor concentrations. Although we use a full inversion of Beer's law in our analysis, we believe that this nonlinearity may arise from near-total attenuation of the beam at high concentrations. We believe this arises from the large variation in u (or B) that occurs at high concentations during a scan across the lineshape. At the concentrations at which we typically work, B does not vary significantly across the scan and it is evaluated at the endpoints only.

We next examine the sensitivity of the laser hygrometer. Figure 4 displays a water vapor absorption spectrum corresponding to a water vapor number density of 2.93×10^{14} molecules cm^{-3} near the lower end of the concentration range of the data in Fig. 3. The signal-to-noise ratio (SNR) of this data is approximately 130:1. This corresponds to an estimated sensitivity of 2.25×10^{12} molecules cm^{-3} with a SNR of 1. For a SNR of 3, the lowest measurable water vapor concentration under these conditions would be 6.75×10^{12} molecules cm^{-3}. The spectrum in Fig. 4 is an average of 200 sweeps acquired at a laser sweep frequency of 200 Hz and with a 9.5-kHz low-pass filter. This implies a detection limit of 9.8×10^{11} molecules $\mathrm{cm}^{-3}\,\mathrm{Hz}^{-1/2}$ with a SNR of 3. The corresponding minimum measurable absorbance is $8.4\times10^{-6}\,\mathrm{Hz}^{-1/2}$. Using the US Standard Atmosphere database [17] and pressure broadening coefficients from the HITRAN 96 database [6], this sensitivity corres-

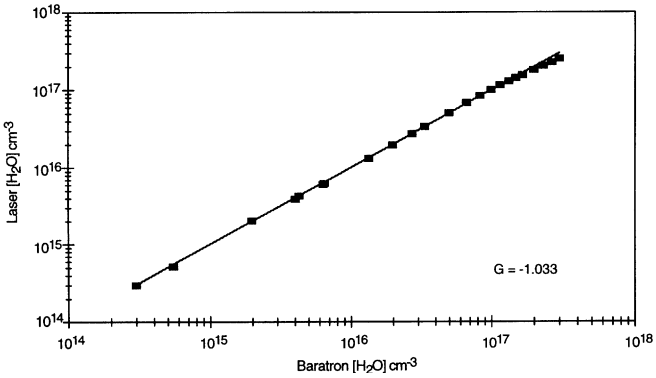

Fig. 3. BRD G-factor calibration plot. G was determined by a linear least-squares fit to the data

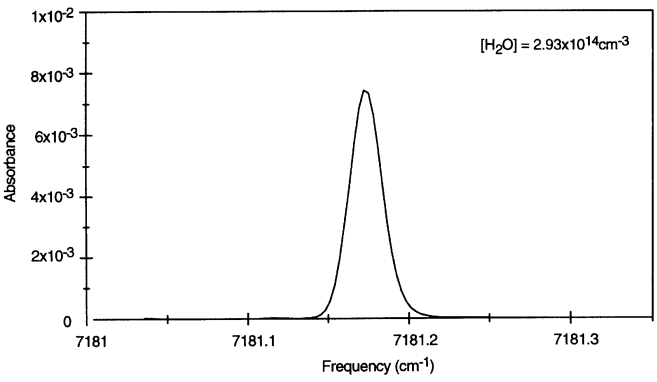

Fig. 4. Water vapor absorption lineshape resulting in a 9.8×10^{11} molecules $\mathrm{cm}^{-3}\,\mathrm{Hz}^{-1/2}$ detection limit

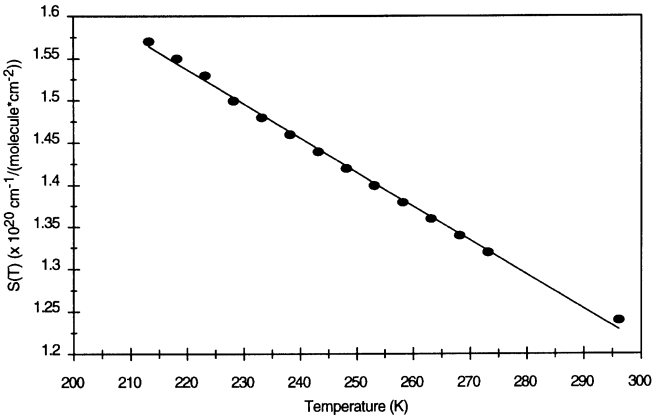

Fig. 5. Measured dependence of $S(T)$ on temperature over the range of 213 to 296 K for the 7181.172 cm^{-1} absorption line of H_2O

ponds to ~ 0.3 ppmv water vapor at typical mid-latitude tropopause conditions[12 km (40 kft)] using a 50-cm absorption pathlength. For comparison, the US Standard Atmosphere water vapor concentration at 12 km is 19 ppmv. Because of increased pressure broadening, the minimum detectable number density for boundary-layer measurements scales to 1.4×10^{13} molecules $cm^{-3}\,Hz^{-1/2}$, which corresponds to 0.6 ppmv (or 2×10^{-3}%RH at 296 K).

We also measured the temperature dependence of the linestrength, S, of the 7181 cm^{-1} absorption line over the range 213 to 296 K. The results are plotted in Fig. 5. The variation in S with temperature is well described by the temperature dependence of the Boltzmann factor and the internal partition function. Our measured value of S is a constant 69% of the value listed in HITRAN over the temperature range of interest. For example, our measured value is $(1.23 \pm 0.046) \times 10^{-20}$ $cm^{-1}/(\text{molecule}\,cm^{-2})$ at 296 K compared to the HITRAN96 value of 1.800×10^{-20} $cm^{-1}/(\text{molecule}\,cm^{-2})$. We have repeated these measurements several times and believe that the HITRAN value is in error. We have used our linestrength temperature dependence in the conversion of measured absorption to number density.

2 Airborne laser hygrometer design

The airborne laser hygrometer has a modular design. It consists of a sensor processor module (SPM) connected to an external air measurement probe via an optoelectronic umbilical. The SPM houses the laser and the system computer. This design ensures environmental control of the laser and provides maximum flexibility in positioning the air measurement probe. The SPM is an industrial-grade, rack-mount computer chassis that also houses the diode laser and its control electronics as well as the BRD and the data acquistion hardware. The SPM requires space for a half-height standard instrumentation rack and weighs on the order of 50 lb. Power requirements are approximately 230 W. The laser is a 1.39-μm DFB device which is internally optically isolated and fiber pigtailed. Temperature and current control for the fiber pigtailed diode laser is achieved by using a single-board OEM controller. The laser produces 1.6 mW output at the fiber pigtail at maximum recommended drive current and a temperature of 26 °C. The fiber-pigtail output from the laser is coupled to a fiber-splitter, providing the signal and reference fiber outputs. The system computer is a single-board 100 MHz Pentium™ device. A 333-kHz data acquistion card, having 32 12-bit differential inputs, is used for data acquisition and control. Three channels are used to monitor the BRD outputs continuously as the laser is scanned, while the remaining input channels are used for monitoring laser setup and control parameters. Four channels are reserved for flight data recording. A 1-MHz analog output is used to create the laser current sweep waveform. Digital outputs from the acquisition board are used to control a programmable amplifier which is incorporated into the BRD. The BRD is mounted directly in the sensor processor module as well. The detectors are large-area (3 mm in diameter), dark-current-matched InGaAs photodiodes mounted within the BRD.

The laser hygrometer has been designed to be a turn-key, stand-alone instrument requiring minimal operator intervention. All aspects of laser control, laser health monitoring, and measurement parameters are fully accessible through the system computer via a graphical user interface written in Labview™ software. Data reduction routines provide for signal averaging of single-sweep absorption spectra followed by baseline subtraction and integration. Data is reported as water vapor number densities. Single absorption spectra are acquired at 100 Hz so that a 10-Hz data reporting rate is obtained after averaging ten individual spectra. The reduced concentration data is continuously streamed to the hard disk.

Ancillary meteorological parameters, measured by other sensors on the aircraft, are sampled by the system computer. These variables include static pressure, differential pressure, total temperature, and dew/frost point. The signals from these sensors are processed internally by the software and are recorded in a log file.

This laser hygrometer uses a unique external air probe for true in-situ measurements. This strategy bypasses extractive sampling issues [7, 11] which can be important in light of the measurement rate of 1 to 10 Hz necessary for high-spatial-resolution measurements from an aircraft traveling at a nominal flight speed of ~ 150 m/s. The external air measurement probe was designed so that the beam is launched from the aircraft fuselage, reflected from a mirror, and returned to a detector in the fuselage. The total optical air pathlength is 50.84 cm. The probe assembly is shown in Fig. 6. The main faring extends 20 cm from the fuselage. The probe was designed so that the measurement volume lies outside the aircraft boundary layer. The beam is carried away from the fuselage before being launched into the ambient air. A launch distance of 20 cm from the fuselage allows the probe to be mounted up to 20 m from the nose of the aircraft. A window block is mounted at the end of the main faring. The windows are fabricated from IR-grade fused silica and are antireflection coated. A corridor in the main faring provides passage for the beams from the fuselage to the window. To account for parasitic absorption in this corridor, the reference beam is also transmitted through the corridor to a mirror at the back of the window, and is reflected to a photodetector inside the fuselage. This volume is also purged during flight. The launch optics and the photodetectors are mounted inside the fuselage. The collimators at the end of the reference and signal beam fibers are gimbaled. Removable cover plates surrounding the interior optics allow access to the components in flight. The distal return mirror is mounted at the end of the mast. The

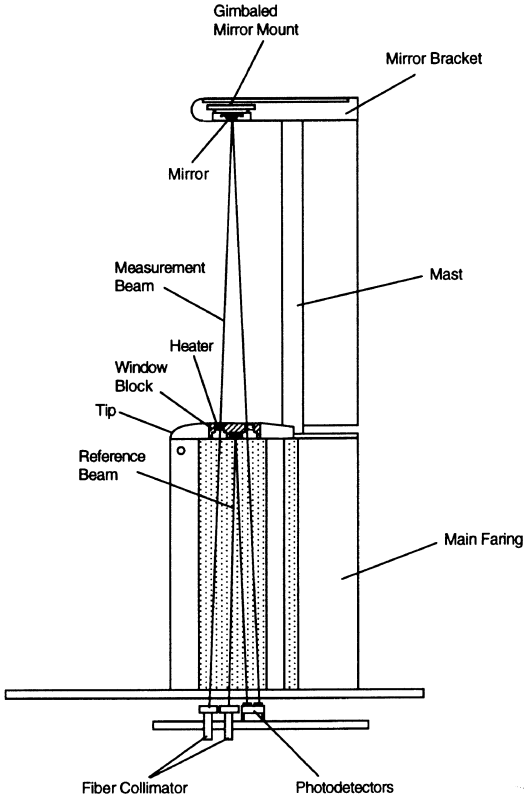

Fig. 6. Probe assembly and optical paths

mirror support was designed to be stiff enough so that aerodynamic loads result in a displacement of the reflected beam on the photodiode of less than 0.21 mm. The return mirror is gimbaled for alignment. The mirrors and windows are heated to prevent condensation.

3 Field demonstration and intercomparison

Airborne operation of the laser hygrometer was demonstrated aboard the NASA P3B research aircraft during the initial phase of the Southern Great Plains Hydrology Experiment based out of Oklahoma City during June 1997. A total of ten flights were made between 18 June and 2 July, 1997. A typical flight pattern involved climbing to 25 kft, and flying four level legs of 280 km in a NNE–SSW pattern with a 80-km offset between legs. The average flight duration was 3.5 hours.

We intercompared the laser hygrometer with two optical chilled mirror (OCM) dew/frost point hygrometers aboard the P3B. These included a General Eastern GE1011 instrument and a Buck Research CR1 instrument. The GE1011 is a standard aircraft instrument that uses a thermoelectric cooler to chill the mirror. The instrument is capable of measuring frost points to −75 °C; however, the dewpoint depression is 55 °C, i.e., the lowest measurable dew point is 55 °C cooler than ambient. The claimed accuracy is ±0.4 to −40 °C and ±1 to −75 °C. The measurement rate is typically 1 Hz. The CR1 is a research-grade instrument that uses liquid nitrogen (LN2) to chill the mirror. The instrument is capable of measuring frost points to −80 °C with an accuracy of ±0.3 °C. The measurement rate is typically 1 Hz but all data presented here have been averaged to 10 s. Both instruments are routinely used aboard the P3B for in-situ measurements of water vapor.

The external air probe of the laser hygrometer was mounted aft of the starboard wing of the P3B on a standard window flange; it was located at a distance of 890 cm from the aircraft nose. The instrumentation rack was located in close proximity to the window flange. This dual rack housed the control instrumentation for the GE1011 hygrometer, the entire CR1 hygrometer, and the sensor processor for the laser hygrometer. LN2 boiloff from the CR1 hygrometer was used to purge the interior volume of the laser probe. The air probe for the CR1 hygrometer was located just below the PSI air probe on the same flange. The GE1011 probe was mounted just aft of the cockpit.

To compare measurements from the two types of instruments, we used the following vapor pressure relations [18, 19] to convert the dew or frost points measured by the chilled mirror hygrometers to number density. Below 0 °C, the water vapor pressure above ice, e_i, is related to the frost point, T_f, by

$$e_\mathrm{i} = \left(1.0003 + 4.18 \times 10^{-6} P_\mathrm{stat}\right) \times 6.1115 \exp\left(22.452 \frac{T_\mathrm{f}}{272.55 + T_\mathrm{f}}\right), \quad (6)$$

where P_stat is the static pressure and both e_i and P_stat are in mB. The number density, $N(\mathrm{cm}^{-3})$, is then calculated from the vapor pressure by using the ideal gas law:

$$N = \frac{1000 e_\mathrm{i}}{1.38 \times 10^{-16} T_\mathrm{stat}}, \quad (7)$$

where T_stat is the static air temperature in °C. For temperatures above 0 °C, the water vapor pressure above liquid water, e_i, is related to the dew point, T_d, by

$$e_\mathrm{i} = \left(1.0007 + 3.46 \times 10^{-6} P_\mathrm{stat}\right) \times 6.1121 \exp\left(17.502 \frac{T_\mathrm{d}}{240.97 + T_\mathrm{d}}\right). \quad (8)$$

The laser hygrometer performed well, providing data at rates to 10 Hz to compare with the chilled mirror instruments which operated at 1 Hz. A comparison of typical flight data from the laser and 1011 hygrometers for level flight conditions at 25 kft is presented in Fig. 7. In this figure, laser hygrometer data at 10 Hz and averaged to 1 Hz are compared with data from the 1011 OCM. The data were collected during flight 1, 14 June, 1997; the static air pressure (SAP) was 376 mb, and the static air temperature (SAT) was 249 K. The greater temporal responsivity of the laser hygrometer is clearly evident by the structure observed in the data between 6300 and 6430 s, which is absent in the OCM data stream. A delay of 10 to 15 s in the OCM data stream with regard to the laser hygrometer data stream is also apparent in the data. The OCM samples air into the aircraft and the observed delay is comparable to the residence time of an air sample flowing through the mirror chamber. Similar data for all three hygrometers for flight 7 at 25 kft are compared in Fig. 8.

The laser hygrometer generally reported somewhat higher water vapor number densities than those calculated from the dew or frost points measured by the chilled mirror instruments. The chilled mirror instruments typically agreed with

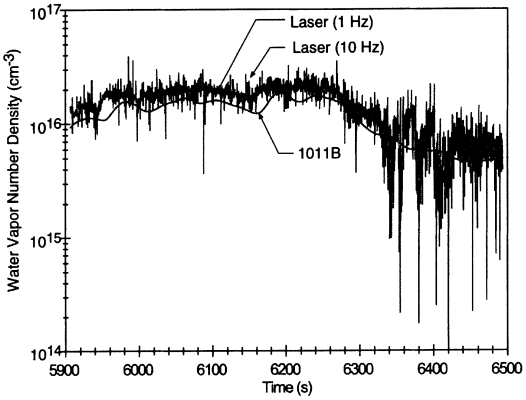

Fig. 7. Comparison of flight data for the laser and GE1011 chilled mirror hygrometer for part of flight 1, 14 June 1997. The altitude was nominally 25 kft, SAT = 249 K, SAP = 376 mB. Data rates were 10 Hz for the laser hygrometer and 1 Hz for the GE1011 hygrometer

one another within error limits (as is shown in Fig. 8) despite the fact that they were located at different points on the aircraft with the CR1 possibly sampling within the aircraft boundary layer. For the data in Figs. 7 and 8, the number density measured by the laser hygrometer is about 20% greater than that reported by the 1011 OCM. This difference between the two types of hygrometers is not well understood at present. We are working to understand this difference via further laboratory and field intercomparisons. One possible explanation is that the water film on the OCM mirror was supercooled. Figure 8 also shows the CR1 number density calculated using (8) instead of (6) and assuming supercooling of the film. As is shown, this assumption leads to better agreement between the laser hygrometer and the CR1 hygrometer.

An example of the spatial structure that can be observed in the water vapor field is illustrated in Fig. 9, which presents data from flight 7 for nominally level flight in clear air at 25 kft for SAT = 252 K and SAP = 377 mB. The aircraft made a turn at 55 880 s and retraced its flight path back through the same airmass. Thus the number density temporal history has a high degree of symmetry around the vertical dotted line at 55 880 s. Spatial structures on the order of 200 s ($\sim$ 30 km) are seen repeated in the number density data stream.

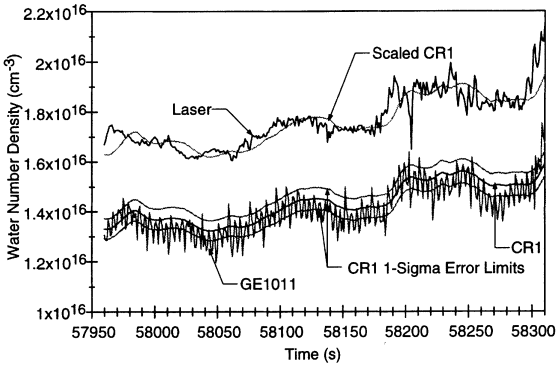

Fig. 8. Comparison of flight data for the laser and both chilled mirror hygrometers for part of flight 7, 25 June. The altitude was nominally 25 kft, SAT = 252 K, SAP = 378 mB. Data rates were 1 Hz for the laser hygrometer, 1 Hz for the GE1011, and 0.1 Hz for the CR1 hygrometer

The temporal response of the laser hygrometer was excellent. Figure 10 is a comparison of data from the laser hygrometer and the CR1 OCM during an encounter with an almost saturated air parcel at 25 kft in much drier air during flight 10. The relative humidity, as calculated from the CR1 data, reached about 80% at the peak of the event. The static air temperature and static air pressure showed only small deviations during the event.

The ultimate sensitivity of the laser hygrometer under field conditions was not determined because of the 25-kft operational altitude. The lowest measured concentration was on the order of 10^{15} molecules cm^{-3} with an SNR of 17 for a 1-Hz measurement. At the corresponding static air temperature and pressure, the corresponding peak absorbance would be 5.5×10^{-3}. The in-situ, pressure-broadened, absorption spectrum displayed undesirable etalon fringes which were not observed in the earlier ground-based testing of the external probe. These fringes limited the minimum measurable number density to approximately 10^{14} molecules cm^{-3}. We are working to identify the optical elements responsible for these etalons so that the full sensitivity identified in the earlier characterization work can be realized in the field.

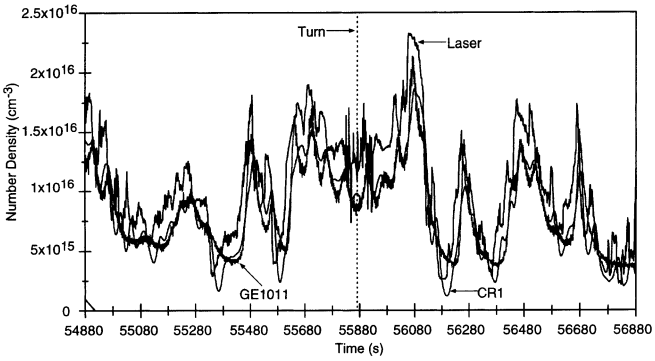

Fig. 9. Comparison of flight data for the laser and chilled mirror hygrometers for part of flight 7, 25 June. The altitude was nominally 25 kft, SAT = 252 K and SAP = 377 mB. The aircraft was halfway through a turn at 55 880 s. Data rates were 1 Hz for the laser hygrometer, 1 Hz for the GE1011, and 0.1 Hz for the CR1 hygrometer

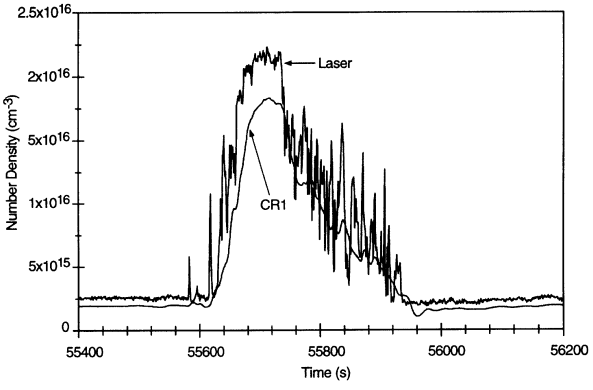

Fig. 10. Comparison of flight data for the laser and CR1 hygrometers for part of flight 10, 29 June. The altitude was nominally 25 kft, SAT = 251 K and SAP = 378 mB. Data rates were 1 Hz for the laser hygrometer and 0.1 Hz for the CR1 hygrometer

4 Future work

We are presently working to increase the measurement rate of the laser hygrometer to better than 20 Hz to enable eddy correlation flux measurements in the boundary layer from an aircraft. Flux measurements are made to characterize the strength of a surface source (or sink) of a trace gas. Airborne demonstration measurements aboard the NASA P3B aircraft are planned for Summer 1998.

We are currently working to reduce the size and weight of the SPM as well as fully automating the sensor. The goal is to create a payload suitable for deployment aboard an unmanned aerial vehicle. In ongoing work for the DOE, we are developing a laser hygrometer payload for the Altus UAV used by the Atmospheric Radiation Measurement (ARM) program. This aircraft has the capability to carry 200-kg payloads to 40 kft and maintain them there for 24 hours. Our laser hygrometer payload is designed to have a weight of 10 kg, including the external air probe, and to require 110 W of power. It will occupy approximately 10% of the available payload volume. The planned integration aboard the aircraft is sketched in Fig. 11.

Future payloads will include capability for near-simultaneous measurement of multiple species. Using wavelength multiplexing, we can combine the output from several lasers onto a single fiber-optic distribution network. By using temporal demultiplexing of the injection current waveforms, a common measurement path and a single photodiode can be used for detection. We have demonstrated near simultaneous detection of CO_2, CH_4 and H_2O by using three fiber-optically coupled lasers as is illustrated in the spectrum of Fig. 12. In this spectrum, the absorbance (in arbitrary units) is plotted against the "data index" which is a measure of frequency. The region over which each individual laser is scanned is indicated along the bottom of the spectrum. Outside the indicated region, a given laser operated at constant current and wavelength. Frequency does not necessarily increase from left to right in the figure. The CH_4 feature at 1.65373 μm is an unresolved triplet in the $2\nu_3$ band. The CO_2 feature at 1.57141 μm is the R(22) line in the $3\nu_1 + \nu_3$ combination band. The H_2O feature at 1.39167 μm is an isolated line in the $2\nu_1 + \nu_3$ combination band. Newly available DFB diode lasers at 2 μm allow access to the strong $2\nu_1 + \nu_3$ combination band of CO_2, in addition to strong lines in the $\nu_2 + \nu_3$ band of H_2O. This will permit sensitive measurements of ambient CO_2 by using pathlengths on the order of a few meters. A spectrum of the R16 line in this band for ambient air at 296 K is presented in Fig. 13. This spectrum indicates the high signal-to-noise ratio achievable with as little as 0.5 m of optical path. The peak absorption is 2.4×10^{-3}.

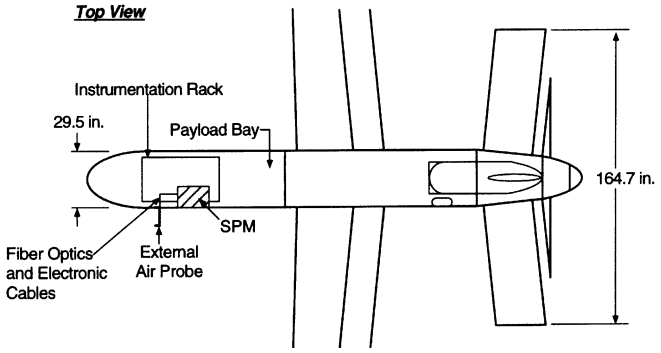

Fig. 11. Schematic diagram of laser hygrometer integration aboard the DOE Altus UAV

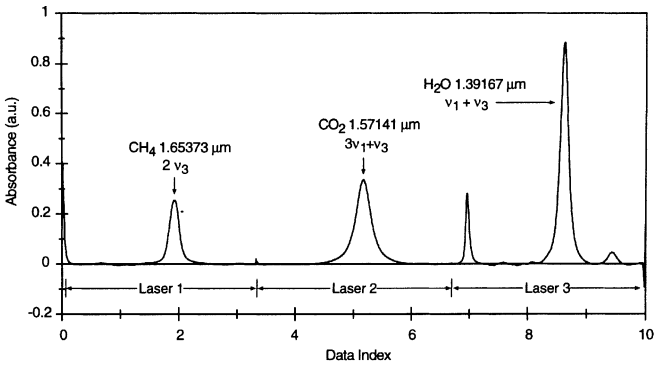

Fig. 12. Baseline-corrected spectrum of CH_4 (0.5 Torr), CO_2 (68 Torr), and H_2O (14 Torr). The spectrum is a 1 s average (100 sweeps at 100 Hz); pathlength 0.5 m, temperature 296 K

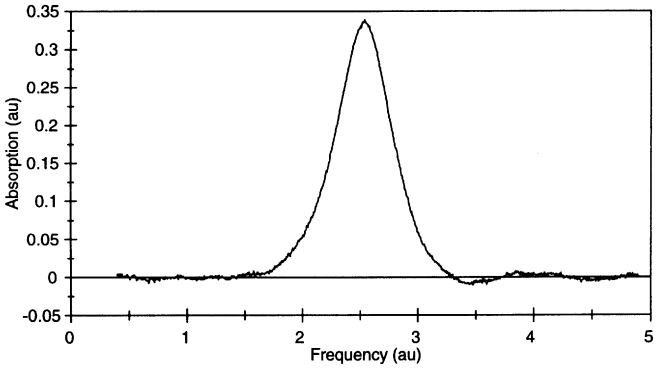

Fig. 13. Absorption spectrum of the R16 line of the (000 → 201) band of CO_2 for ambient lab air at 296 K and 0.5 m pathlength

5 Conclusion

We have developed a near-IR diode laser hygrometer for in-situ measurement of tropospheric water vapor from aircraft. The sensor uses an external optical measurement path defined by using a symmetric airfoil for true in-situ sensing of free-stream air beyond the boundary layer of the aircraft. The laser hygrometer has a 10 Hz measurement rate and a dynamic range greater than three decades. It is capable of measuring ambient water vapor levels from the Earth's boundary layer to the tropopause. Based on extensive laboratory testing, the laser hygrometer has a predicted sensitivity of 10^{12} molecules cm^{-3}. This sensitivity corresponds to approximately 0.3 ppmv water vapor at typical mid-latitude tropopause conditions. Because of pressure broadening, the minimum detectable number density for boundary layer measurements is 10^{13} molecules cm^{-3}, which corresponds to 0.6 ppmv at 1 atm and 296 K. The laser hygrometer was deployed aboard the NASA P3B research aircraft and demonstrated over a series of flights during the summer of 1997. It was successfully intercompared with two optical chilled mirror hygrometers. An improved version of the sensor will undergo further flight testing during the summer of

1998. A downsized and fully automated version of the sensor is being developed for deployment on unmanned aerial vehicles.

Acknowledgements. We wish to acknowledge the many contributions from Phil Mulhall of Physical Sciences Inc. to this work. This work was supported by the NASA Langley Research Center and Department of Energy under the SBIR program.

References

1. G.M. Stokes, S.E. Schwartz: Bull. Am. Meteorol. Soc. **75**, 1201 (1994)
2. N. Nicholls, G.V. Gruza, J. Jouzel, T.R. Karl, L.A. Ogallo, D.E. Parker: In *Climate Change 1995, The Science of Climate Change*, ed. by J.T. Houghton, L.G. Meira Filho, B.A. Callander, N. Harris, A. Kattenberg, K. Maskell (Cambridge University Press, New York 1996) Chap. 3
3. S.J. Oltmans, D.J. Hofmann: Nature **374**, 146 (1995)
4. A.J. Hills, R.J. Fleming: *Commercial Aviation Sensing Humidity (CASH) Sensor Evaluation Phase Final Report* (National Oceanic and Atmospheric Administration 1994)
5. Buck Research, Boulder, CO
6. L.S. Rothman, R.R. Gamache, R.H. Tipping, C.P. Rinsland, M.A.H. Smith, D. Chris Benner, V. Malathy Devi, J.-M. Flaud, C. Camy-Peyret, A. Perrin, A. Goldman, S.T. Massie, L.R. Brown, R.A. Toth: J. Quant. Spectrosc. Radiat. Transfer **48**, 469 (1992)
7. J.A. Silver, A.C. Stanton: Appl. Opt. **26**, 2558 (1987)
8. C.R. Webster, R.D. May, C.A. Trimble, R.G. Chave, J. Kendall: Appl. Opt. **33**, 454 (1994)
9. J. Podolske, M. Loewenstein: Appl. Opt. **32**, 5324 (1993)
10. M. Loewenstein: The Perseus Data Link **1**, 2 (1993)
11. J.A. Silver, D.C. Hovde: Rev. Sci. Instrum. **65**, 1691 (1994)
12. J.E. Collins, Jr, G.W. Sachse, L.G. Burney, L.O. Wade: Atmospheric Effects of Aviation Project, 5th Annual Meeting, Virginia Beach, VA, April 23-28, 1995
13. P.C.D. Hobbs: Appl. Opt. **36**, 903 (1997)
14. K.L. Haller, P.C.D. Hobbs: Quant. Spectrosc., Proc. SPIE **1435**, 298 (1991)
15. P.C.D. Hobbs: Proc. SPIE **1376**, Laser Noise, 216 (1991)
16. M.G. Allen, K.L. Carleton, S.J. Davis, W.J. Kessler, C.E. Otis, D.A. Palombo, D.M. Sonnenfroh: Appl. Opt. **34**, 3240 (1995)
17. U.S. Standard Atmosphere, 1976 (National Oceanic and Atmospheric Administration, National Aeronautics and Space Administration, U.S. Air Force, Washington, DC 1976
18. General Eastern Instruments, Woburn, MA
19. A. Buck: J. Appl. Met. **20**, 1527 (1981)